ADVANCED ELECTRONIC MATERIALS Open Access
www.advelectronicmat.de

Open-Source Tools for the Fabrication and Characterization of Organic Electronics

*Julian F. Butscher, Seonil Kwon, Anna Popczyk, and Malte C. Gather**

By promoting collaborative sharing of knowledge, the open-source movement has catalyzed substantial progress across diverse fields, including software development and artificial intelligence. Similarly, the concept of openly shared hardware has gained attention, due to its cost-effectiveness and the prospect of improved reproducibility. A major motivation for the development of organic electronics is its promise to deliver substantial advantages in price and manufacturability relative to its inorganic counterpart. Here, two open-source tools for organic electronics are introduced: a dip-coating device designed for thin film fabrication and a four-point probe for precisely measuring the resistance of thin films. These tools only cost a fraction of comparable commercial devices and run with open-source software to ensure a user-friendly experience. A case study demonstrates the optimization of simple fluorescent organic light-emitting diodes (OLEDs) using these open-source tools achieving 4% external quantum efficiency (EQE). To characterize these OLEDs, a previously reported open-source setup for accurate efficiency measurements is used. A substantial software upgrade to this setup, which speeds up the characterization of electroluminescence, is also repor. This work contributes open-source hardware and software to the field of organic electronics, thereby lowering the entrance barrier to the field and fostering the involvement of scientists with diverse scientific backgrounds.

1. Introduction

Through collaborative sharing of designs, software, and methodologies, open-source initiatives have democratized scientific endeavors and thus empowered researchers across disciplines to contribute, replicate, and actively participate in expanding existing knowledge. Notably, this cooperative model has gained substantial attention in the field of open-source generative artificial intelligence.[1–3] Hardware tools that follow a similar ethos have also captured growing interest, and have been a driving force in promoting collaboration, enhancing accessibility, and fueling innovation.[4–7] They offer cost-effective alternatives, often utilizing affordable components, 3D-printed parts, and readily available materials, thus allowing researchers from diverse scientific communities worldwide to experiment, prototype, and optimize fabrication processes without the burden of prohibitive cost. Additionally, through the detailed documentation of open-source equipment, experimental reproducibility can be enhanced. [8]

Organic electronic devices promise significant advantages over their inorganic counterparts due to the relatively cost-effective synthesis of the involved materials and their ease of manufacturing. Organic light-emitting diodes (OLEDs) are the workhorse of organic electronics and have revolutionized the display and lighting industries with their exceptional characteristics, including self-emission, wide viewing angles,[9] and intrinsic mechanical flexibility.[10,11] They can be manufactured via thermal evaporation of the constituting layers in a vacuum or from solution. While thermal evaporation usually yields higher purity films and thus is often associated with better device stability, solution processing is of great interest due to its simplicity and cost-effectiveness.[12] Dip coating, in particular, provides a simple, affordable, and versatile method to fabricate thin films on flat surfaces as well as on more complex topologies, and unlike spin-coating promises reasonable scalability to both high throughput and large substrates.[13] Furthermore, for material deposition from low-viscosity solutions, dip coating can offer a versatile platform to deposit thick layers in a single deposition step.[14]

Dip coating involves immersing a substrate into a solution of the desired material, followed by controlled withdrawal of the

J. F. Butscher, M. C. Gather
Organic Semiconductor Centre
SUPA
School of Physics and Astronomy
University of St Andrews
St Andrews KY16 9SS, UK
E-mail: malte.gather@uni-koeln.de
J. F. Butscher, S. Kwon, A. Popczyk, M. C. Gather
Humboldt Centre for Nano- and Biophotonics
Department of Chemistry
University of Cologne
50939 Cologne, Germany

The ORCID identification number(s) for the author(s) of this article can be found under https://doi.org/10.1002/aelm.202400460

DOI: 10.1002/aelm.202400460

substrate and subsequent drying of the wet film formed on the surface of the substrate. It has been used for the fabrication of many different structures and devices, such as OLEDs—, e.g., on textile fibers,—[15] distributed Bragg reflectors (DBRs),[16] and electrodes.[17–19] While dip coating is a simple technique in principle, its more widespread application in research laboratories is in part still prevented by the significant cost of commercial dip coaters, which often cost thousands of euros/dollars.

The fabrication of organic electronics invariably involves the deposition of thin film electrodes capable of carrying current over considerable distances with minimal losses. These electrodes are mainly characterized by their surface roughness, optical transparency, and sheet resistance.[20,21] A simple, yet accurate technique to determine the sheet resistance of thin films is the four-point probe.[22] As the name suggests, this method uses four probes, often arranged in a linear configuration, to make electrical contact with the targeted layer. By applying a current through the outermost pair of probes and measuring the voltage drop across the two inner probes, the resistance can be determined, without the need to account for internal or contact resistances as is required for two-point experiments. While the principle of this technique is strikingly simple, again, commercial probing systems often cost several hundreds to thousands of euros.

Ultimately, the performance of the final OLED stack is the determining criterion in evaluating organic electronic devices; therefore, they must be evaluated in a controlled and reproducible way. We recently reported on an open-source alternative for accurate efficiency measurements of OLEDs. Our system accounts for the angular emission characteristics of OLEDs to arrive at correct values for device efficiency, which is particularly important for complex OLED designs, such as microcavity OLEDs, where the angular distribution of the radiant intensity can differ significantly from the ideal Lambertian emission profile.[23,24] However, the accessibility and throughput of our former system were somewhat hampered by the lack of an easy-to-use user interface.

This work shares an upgrade to our previously reported angle-resolved electroluminescence (AR-EL) characterization setup [24] as well as two novel open-source hardware projects; these are a dip coating device for thin film fabrication as well as a four-point probe for the characterization of conductive thin films. Both hardware devices are fabricated from readily available or 3D printable components, are compact enough for and compatible with operation inside a nitrogen glovebox, and run with custom, openly shared software. Indeed, the provided software packages represent a substantial part of the discussed work. The overall cost of the basic components is ≈70 euros for the dip coater and less than 30 euros for the four-point probe. We use the dip coater developed in this work to deposit thin films of PEDOT:PSS and of the Poly(p-phenylen-vinylene) derivative Super Yellow (SY-PPV) of varying thicknesses and analyze the quality of the fabricated films. Furthermore, we show an optimization of the conductivity of two representative thin film electrodes—aluminum-doped zinc-oxide (ZnO:Al) and silver—using our four-point probe. Lastly, we bring both results together by fabricating simple OLEDs with dip-coated organic layers in both bottom-emitting and semi-transparent configurations. Using our previously presented AR-EL characterization setup with the newly programmed control interface, we find that the external quantum efficiencies (EQEs) of these OLEDs reach up to 4%, in line with the expected value for a fluorescent, solution-processed device. This work aims to contribute to the expansion of the repertoire of open-source tools for the fabrication and characterization of organic electronic devices and, therefore, to foster accessibility, reproducibility, and collaboration among scientists in our field and beyond.

2. Result

2.1. Overview

A typical workflow for the fabrication of organic electronic devices is summarized in the flow chart illustrated in **Figure 1a**. Usually, the process starts with the deposition of single layers to optimize the coating parameters. In this work, we present a dip-coating device that can be used for this step requiring the optimization of retraction speed, retention time, and solution concentration (Figure 1b). The resulting films are subsequently characterized using various methods such as profilometry, to determine the thickness of the films, and atomic force microscopy (AFM) to determine the uniformity of the film on the micrometer scale. While the bottom electrode for such devices is often prepatterned indium tin oxide (ITO), the top electrode must be deposited subsequently. Optimization of the top electrode for, e.g., transparency, uniformity, and conductivity is usually carried out separately. We present a four-point probe that can be used for the investigation of the sheet resistance of such thin films (Figure 1c). Lastly, the optimized layers are brought together to fabricate a full device that can then be characterized and optimized further. For the characterization of the electroluminescent properties of an exemplary OLED, we also show an upgrade to our previously reported AR-EL characterization setup (Figure 1d).[24] This manuscript presents the devices by guiding through the flow chart of fabricating OLEDs starting with our dip coater design to deposit organic thin films, continuing with thin film characterization using our four-point probe, and finally discussing the characterization of OLEDs with the newly provided open-source software packages.

2.2. Film Fabrication (Open-Source Dip Coater)

Dip-coating represents a very simple technique, nevertheless, several requirements must be fulfilled to enable consistent fabrication of high-quality thin films. These include minimizing vibration as well as ensuring smooth retraction at defined speeds.[25] To match these requirements, we developed a simple device that can be built from easily accessible and inexpensive components. Our dip coater is built around a NEMA17 stepper motor controlled by an Arduino Nano and a DRV8825 stepper motor module (schematics of the electronics can be found in Figure S1, Supporting Information). We chose a stepper motor in this project instead of a DC servomotor due to its significantly lower cost. No significant motor heating was observed, as the motor is kept in an idle state when it is not moving. The user interacts with the device using a rotary encoder and a 16 × 2 digit LCD display (**Figure 2a**). This combination allows for intuitive

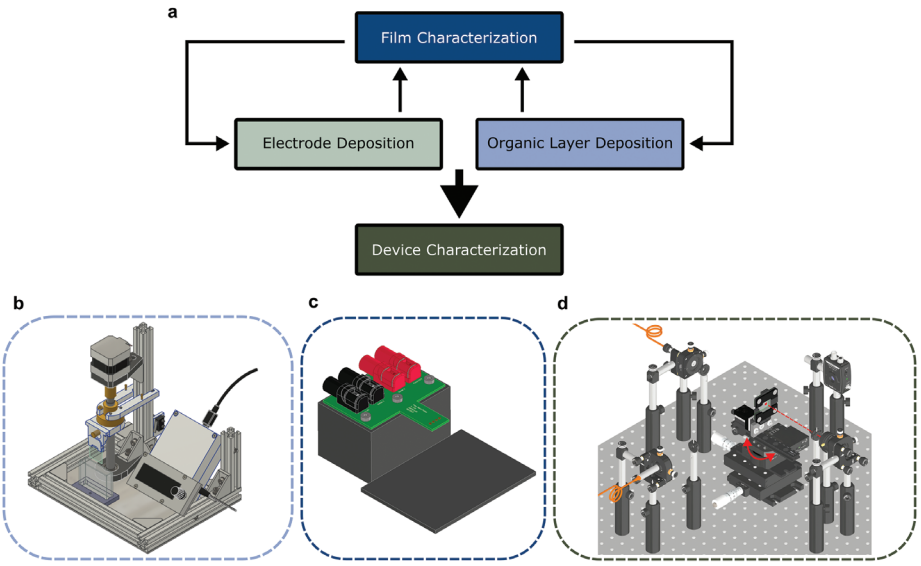

Figure 1. a) Flow chart for the fabrication of organic electronic devices. Thin film organic layers as well as electrodes are deposited via, e.g., dip coating or thermal evaporation. The thin film layers are characterized for thickness, morphology, and electrical properties (e.g., using a four-point probe) until the desired properties are found. Finally, the optimized organic and electrode layers are combined in an actual device that is characterized and optimized further (e.g., for their electroluminescence properties in the case of an OLED). In this work we present a dip coating device b) for thin film fabrication, a four-point probe c) for sheet resistance measurements (film characterization), and an upgraded version of our previously presented electroluminescence characterization setup (device characterization)[24] d).

and easy handling, even when the device is placed inside a glovebox.

The rotations of the stepper motor are transformed to linear motion through a spindle drive. This principle is used in many industrial applications, such as 3D printing, and allows for cost-effective and precise movement. The lead screw is held by two aluminum rods lubricated by two PTFE pads to reduce friction. Stepper motors divide each revolution into a defined number of steps. Depending on the lead pitch of the used spindle, the linear motion can be controlled with micrometer accuracy. For the chosen lead pitch (2 mm) and our stepper motor, which has 200 steps/revolution, each step corresponds to ≈10 µm of linear motion. By default, the user interface works with units of steps, the corresponding motion in units such as mm s^{-1} can be calculated from the above considerations or an additional calibration measurement. Furthermore, as the DRV8825 stepper motor driver allows for up to 32 micro steps per actual step, the resolution could be improved further; however, we do not expect that this is needed for most dip-coating applications. A step-by-step guide for the assembly of the device can be found in the Supporting Information. The full CAD drawings of the system are provided via the University of St Andrews Repository https://doi.org/10.17630/651679f3-4d56-40cd-b6da-e0c24804bcc3 and a complete part list can be found in Table S1 (Supporting Information).

When the dip coater is started by connecting it to a 12 V power supply, it first moves downward until it hits a microswitch to calibrate its zero position. After successful calibration, the user sees the main menu (Figure 2b). The menu allows for 1) manual movement (turning the rotary encoder will move the dip coater up or down), 2) the selection of one of three adjustable saved dip-coating recipes, and 3) changing of the settings, such as the micro stepping settings. After selecting one of the three programs, the user can change the top position, bottom position, speed, acceleration, and retention time of the dip coating process. The settings are stored in the nonvolatile EEPROM storage of the Arduino, which is maintained even after disconnecting the dip coater from power. A full description of the dip coater menu can be found in Figure S2 (Supporting Information).

To showcase the utility of the dip coater, we fabricated PEDOT:PSS films using a series of different retraction speeds (Figure 2c). For retraction speeds between 2.7 and 3.7 mm s^{-1}, the resulting films had good long-range uniformity whereas the PEDOT:PSS layers produced at a retraction speed of 6.2 mm s^{-1} showed a more inhomogeneous surface topology. The high quality of the dip-coated layers was further confirmed by AFM measurements (Figure 2d) showing a root mean square roughness (R_q) of less than 1.5 nm for a retraction speed of 2.7 mm s^{-1}. Furthermore, even with a 20 µm × 20 µm field of view, corresponding to the linear motion covered by at least two motor steps, no ripples are introduced on the dip-coated film as confirmed by a large-scale AFM measurement (Figure S3a, Supporting Information). Figure 2e shows the film thickness as a function of the retraction speed for films of PEDOT:PSS and SY-PPV. For faster retractions, we observed an increase in film thickness as expected from Landau–Levich theory.[26,27] An AFM micrograph of a 70 nm thick SY-PPV film confirming its high quality and low roughness of R_q = 0.5 nm is shown in Figure S3b (Supporting Information).

2.3. Determination of Electrode Resistance (Open-Source Four Point-Probe)

According to Ohm's law, electrical resistance can be measured by simply dividing the applied voltage by the flowing current.

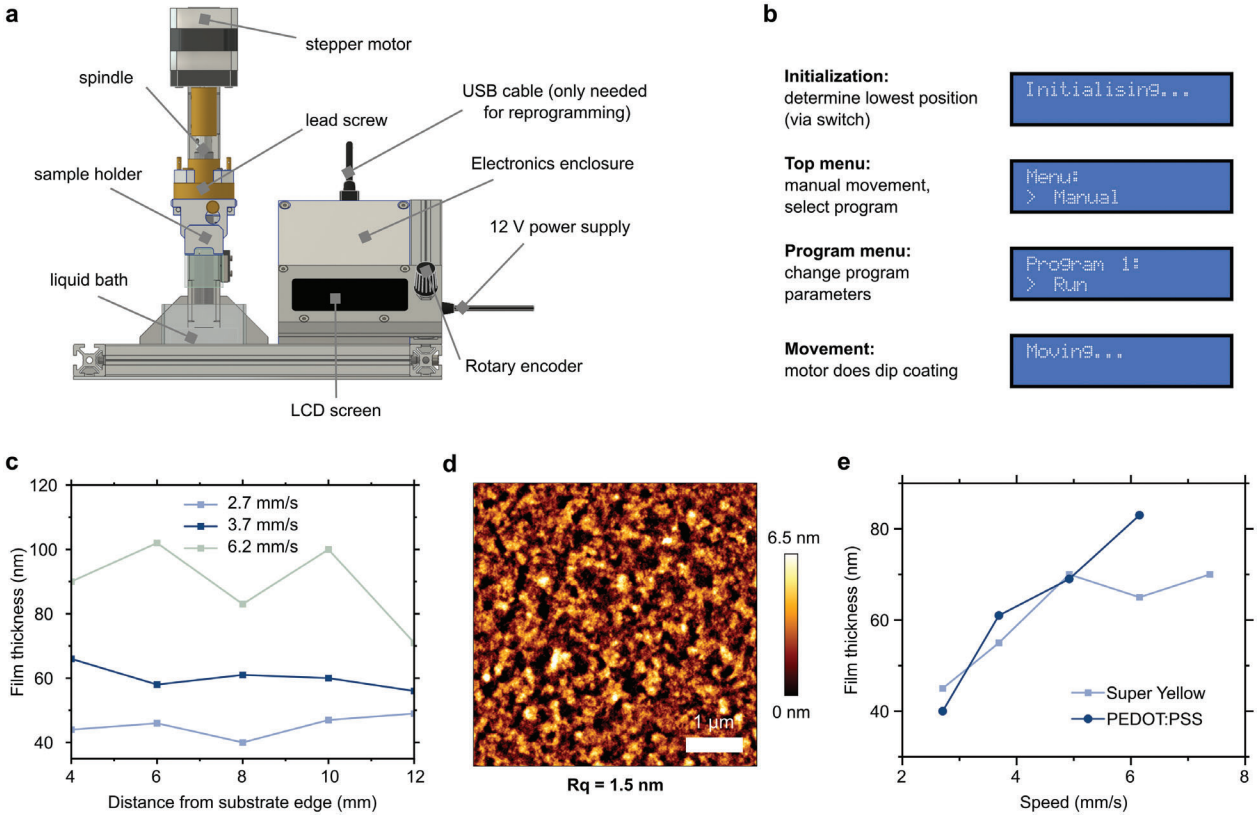

Figure 2. a) 3D rendering of open-source dip-coater (front view). The dip-coater is based on a spindle drive coupled to a NEMA17 stepper motor. The lead screw transforms the rotation of the spindle into a linear motion and carries a sample holder with the substrate. The electronics to drive the stepper motor and receive user input are encased in the electronic enclosure. The user menu is displayed via 16 × 2 digit LCD screen that can be navigated via a rotary encoder. b) A custom user interface running on the controlling Arduino Nano allows for direct interaction with the device. Three different dip coating recipes can be programmed and stored. c) Uniformity of PEDOT:PSS films on glass deposited via dip coating at different retraction speeds. d) AFM micrograph of a 45 nm thick PEDOT:PSS film fabricated with 2.7 mm s^{-1} retraction speed on glass. Rq denotes the root mean square roughness. e) Thickness of films of SY-PPV and PEDOT:PSS prepared at different retraction speeds.

However, for an accurate measurement, it is vital to ensure that no parasitic resistances, such as wire or contact resistances, distort the measurement. A simple, yet effective way of achieving this, is to use a four-point probe, which separates the applied current from the measured voltage drop. While the absolute resistance of a sample is the important factor for its performance, resistivity is defined to evaluate the efficiency of a material to conduct current in a geometry-independent way. Additionally, for 2D materials, the sheet resistance can be a valuable quantity to assess the conductivity of thin films and compare their absolute conductivity regardless of their thickness (e.g., as in the case of silver electrode optimization below). To calculate resistivity and sheet resistance, several geometric parameters must be considered. These parameters are most easily accounted for using lookup tables for different geometries, as the determination of geometrical parameters can be a complex task.[28]

From geometrical considerations for evenly spaced probes, the sheet resistance measured by a four-point probe is given by Equation (1).

$$R_s = \frac{\pi}{\log(2)} \times \frac{V}{I} \times C_{\text{thickness}} \times C_{\text{width}} \quad (1)$$

where I is the applied current, V is the measured voltage drop, $C_{\text{thickness}}$ the finite thickness correction factor, and C_{width} the finite width correction factor. The derivation of the above formula as well as a list of correction factors for a variety of different geometries can be found in Ref. [29].

Here, we demonstrate a simple, yet user-friendly and accurate four point-probe based on readily available components that can be purchased for less than 30 euros at the time of writing (plus some further standard equipment available in most laboratories as explained below). The design of our four-point probe is shown in **Figure 3**a; it consists of a printed circuit board (PCB) with spring-loaded gold contact pins and four banana plug adapters to easily connect to a current source and a multimeter. The schematic of the PCB can be found in Figure S4 (Supporting Information), the corresponding Gerber files, which can be used to order the PCB from a manufacturer, as well as full CAD drawings, are again shared via the University of St Andrews Repository (https://doi.org/10.17630/651679f3-4d56-40cd-b6da-e0c24804bcc3)-. The PCB is mounted on a 3D printed holder so that a z-stage and the sample under investigation can be placed underneath the gold pins. The z-stage is necessary to make contact between the sample and the four-point probe, which sits at a fixed height. Most z-stages can be used for this task as there

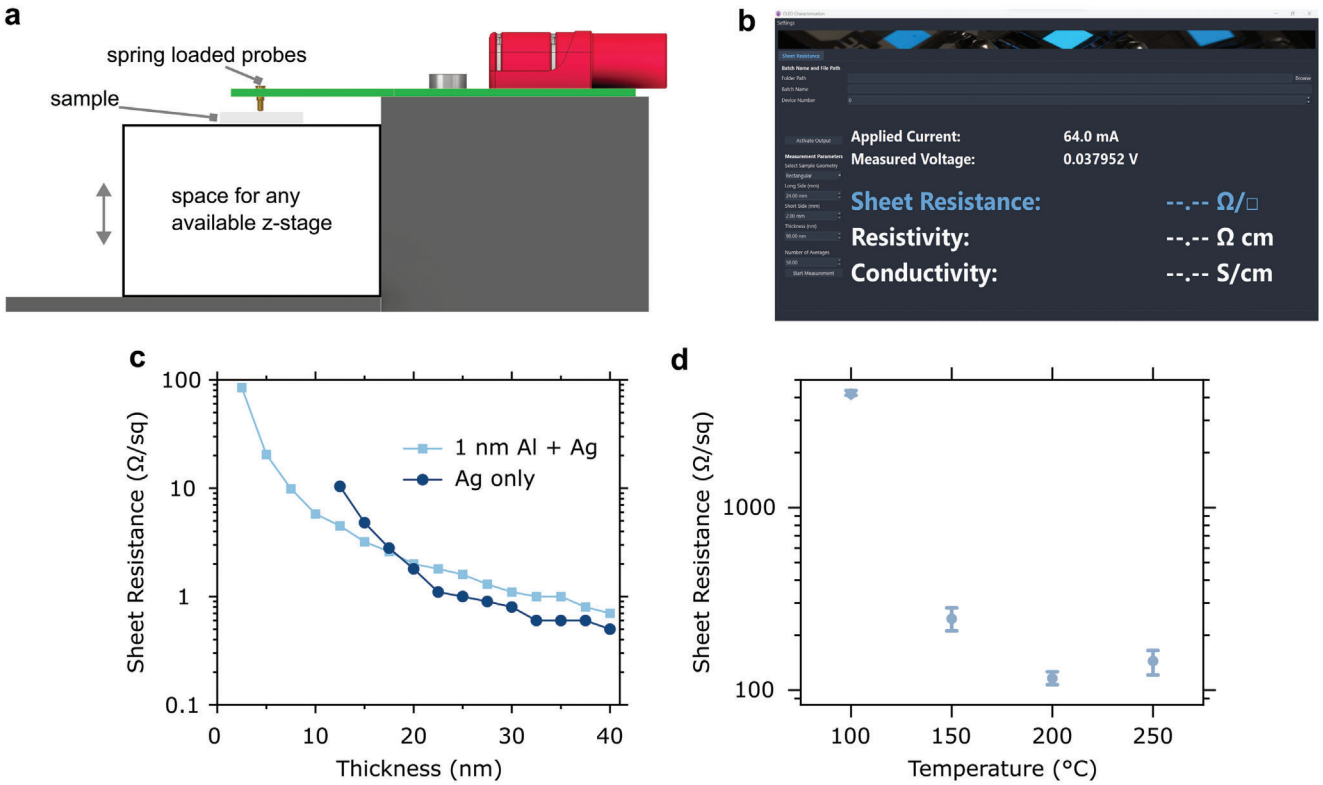

Figure 3. a) Schematic side view of the four-point probe consisting of a custom printed circuit board, four banana plug adapters, and four spring-loaded gold pins. The sample is mounted from the bottom from where it is lifted into position with a z-stage. b) Open-source user software to control the current source and voltmeter. Conversion to sheet resistance, resistivity, and conductivity is done based on the sample dimensions provided by the user. c) Conductivity measurements of thermally evaporated silver films with (light blue) and without (dark blue) aluminum seed layer. d) Optimization of sheet resistance of transparent conductive oxide electrode of ZnO:Al deposited via atomic layer deposition at different temperatures.

is no demanding requirement for z-resolution. A full list of required materials, including a possible z-stage, is given in Table S2 (Supporting Information.

We provide a simple open-source software (Figure 3b) that allows for automatic control and calculation of the sheet resistance from the applied current and the measured voltage drop as well as geometric parameters provided by the user (GitHub: https://doi.org/10.5281/zenodo.12722101). We used a Keithley Sourcemeter 2450 as the current source and a Keithley Multimeter 2100 as the voltmeter, the same instruments we recommended for use with our previously developed AR-EL characterization setup.[24] However, any equipment compatible with Standard Commands for Programmable Instruments (SCPI) communication and sufficient resolution can be used, as the software can be easily adapted to other hardware.

To test our four-point probe, we investigated the sheet resistance of two common electrode materials available in our lab, the transparent conductive oxide (TCO) aluminum-doped zinc-oxide (ZnO:Al), which we deposited via atomic layer deposition (ALD), and silver, which was deposited via thermal evaporation. Figure 3c shows the sheet resistance of silvers of different thicknesses deposited with and without a 1 nm thick aluminum seed layer. In both cases, the sheet resistance initially decreases rapidly with increasing film thickness and then converges toward the bulk value of silver for higher thicknesses. The nonlinear decrease in sheet resistance with thickness can be attributed to the growth behavior of silver. Without the aluminum seed layer, we were only able to determine a sensible sheet resistance starting from a film thickness of 12.5 nm, which we attribute to silver showing pronounced island growth on the bare glass.[21] In line with reports in the literature, silver films without the aluminum seed layer reach a slightly lower sheet resistance in the large film thickness limit.[21]

Furthermore, Figure 3d shows the optimization of the sheet resistance for ZnO:Al deposited via ALD at different temperatures and with otherwise fixed deposition parameters (see Experimental Section). The sheet resistance initially reduces with increasing temperature and reaches an optimum at 200 °C before it starts to increase again. Since the resistivity should further decrease for higher temperatures,[30] we attribute the increase in sheet resistance to a reduced growth rate for higher temperature ZnO processes.[20]

2.4. Electroluminescence Characterization (User Interface for Open-Source EL Setup)

Next, the previously optimized film deposition recipes were used to fabricate a simple OLED based on PEDOT:PSS as the hole transport layer and SY-PPV as an emitter.[31] We fabricated two different device structures, a semi-transparent device with a highly conductive yet semitransparent 20 nm thick silver top

contact, seeded with a 1 nm aluminum layer as discussed above, and a bottom-emitting device with an opaque 100 nm thick aluminum top electrode.

To characterize OLEDs, we previously described a custom goniometer setup that allows accurate characterization of electroluminescence via AR-EL measurements.[24] The hardware configuration and the calculations underlying the analysis of the AR-EL measurements are described in detail in our previous report and thus are only summarized briefly. The setup consists of a motorized goniometer stage for mounting the OLED, a calibrated photodiode with an integrated amplifier, and a fiber spectrometer. First, the goniometer is rotated such that the OLED faces the photodiode, which is positioned at a sufficient distance from the OLED to cover a negligible angle range and thus only record light emitted perpendicular to the device surface (forward direction). The voltage applied to the OLED is ramped up in user-defined steps and the current through the device as well as the photocurrent picked up by the photodiode are recorded. Subsequently, the OLED is rotated, and the electroluminescence spectrum is recorded as a function of emission angle using the fiber spectrometer. While the system described in our earlier report allowed for accurate and robust device characterization, it lacked a user-friendly software interface for measurement and data analysis. Therefore, we now developed a completely new software package, consisting of characterization software (available via GitHub: https://doi.org/10.5281/zenodo.10546513) that interfaces with the hardware to perform the actual measurement, and an evaluation software that allows for the automated evaluation of the data within seconds (available via GitHub: https://doi.org/10.5281/zenodo.10546515). To showcase the features of both pieces of software, the characterization of the two device structures introduced above is described in the following.

The suggested workflows for the measurements as well as for the evaluation of the data are summarized in Figures S6 and S7 (Supporting Information). After mounting the sample, the user starts with defining a folder path for data storage and adds some additional metadata such as device number and batch name for later reference. Current-voltage characteristics of the OLED pixels are subsequently recorded alongside the photodiode voltage, which will later be converted into photometric and radiometric quantities. If the auto position option is selected, the goniometer motor automatically turns the OLED toward the photodiode for the measurements, subsequently selects the brightest pixels, and then turns the OLED toward the spectrometer. The software then switches to the spectrum tab, where the user can adjust applied voltage and integration time before recording an electroluminescence spectrum together with a dark spectrum for background subtraction to file.

For OLEDs with a non-Lambertian emission, it is vital to account for the angular dispersion of the emission. In addition to recording a forward spectrum, the user can select the goniometer tab, where they can again adjust the measurement parameters, such as the angle increment between spectra, applied current, and integration time. As previously described by Archer et al.,[24] the motor then moves to different angles, thereby recording the angular emission characteristics of the device. The new interface allows the plotting of the data in real-time (**Figure 4** top) and enables direct user feedback, which is important as this is the most time-consuming part of the electroluminescence characterization. For instance, an asymmetry of the maximum intensity can indicate a misalignment of the sample which can be corrected even before the measurement is completed.

Furthermore, we introduce an additional feature for OLEDs with poor operational stability, namely a degradation check (Figure 4 bottom). When this option is selected, the software takes an additional spectrum in the forward direction before and after the measurement. The difference between the maxima of the peaks is a reasonable indication of the amount of degradation during the measurement itself (The typical cumulated on-time of an OLED for a complete angular dispersion measurement is 90 s or more; the total on-time is saved to file after each measurement). The software then saves the angle-resolved spectrum in a noncorrected format and stores a version that is corrected for the degradation of the device. For this, the software assumes an exponential decay of the OLED brightness I according to Equation (2).

$$I\ (i) = I_0\ e^{-\lambda i} \tag{2}$$

where i represents the i-th angle step, N is the last angle step, and $\lambda = -\frac{1}{N}\ln(\frac{I_N}{I_0})$ is a degradation time constant. While a stretched exponential decay might give a more accurate description of the decay characteristics, the beta parameter of the stretched exponential cannot be fitted with two available data points, and thus such a correction would require a separate measurement of device stability, which in our view adds too much complexity to the presented system.[32,33]

To quickly convert the raw data to photometric and radiometric quantities, we developed an evaluation software that guides the user through the process of evaluating and accessing their data (**Figure 5**). The full evaluation process is thoroughly described in Figure S7 (Supporting Information). In addition to the recorded data, the software needs some information about the geometry of the sample (active area) and the measurement setup (distance between OLED and photodiode). After entering these parameters, a folder containing the raw data can be selected. The file names of all files in that folder are extracted and devices available for evaluation are listed (Figure 5 bottom left). Devices can be assigned to a group of devices that share the same emission spectrum and angular dispersion. Only now is the data converted to photometric and radiometric quantities. The user can plot the JVL curves of the different devices and sort out unreasonable curves (e.g., defective pixels) by clicking on the according color in the legend (Figure 5 bottom right).

For an easy comparison of the performance of different groups, the user can plot performance statistics (Figure 5 top). For our example series of opaque bottom emitting devices, we immediately see which dip-coating parameters lead to the best performance. Furthermore, the statistics show the good reproducibility we can obtain when using our custom-made dip-coating device to fabricate an OLED stack. The best EQEs, for instance, are obtained for devices coated with retraction speeds of ≈3 mm s^{-1} for the PEDOT layer and ≈7 mm s^{-1} for the SY-PPV layer. Under these conditions, a maximum EQE of ≈4% is reached, with a median EQE of 3.7% for multiple devices. These results agree well with EQEs reported in the literature on OLEDs manufactured via spin-coating using commercial devices.[2,33,34]

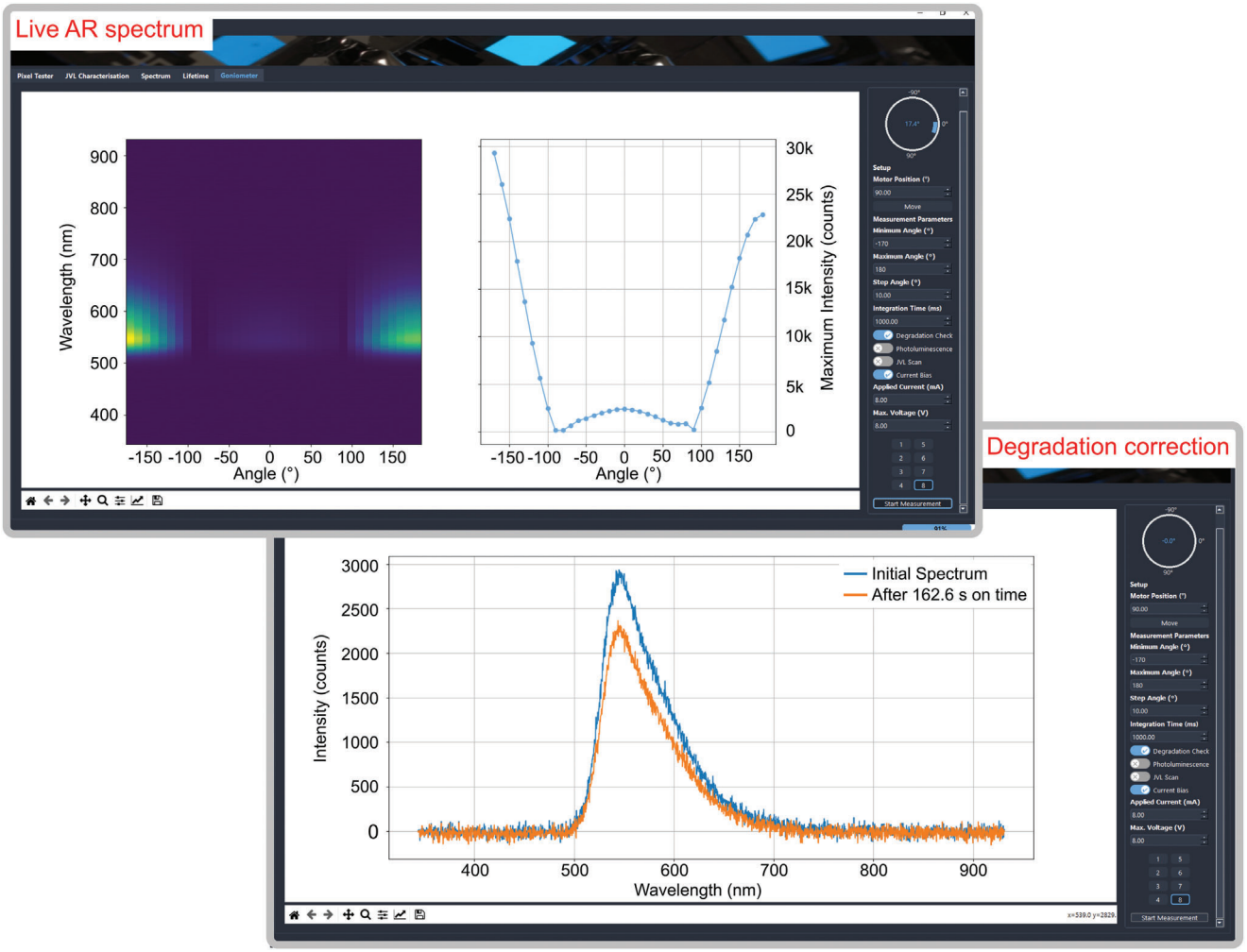

Figure 4. Characterization software for the electroluminescent characterization of OLEDs using our previously described setup. Here, the measurement of an angle-resolved electroluminescence spectrum is shown directly displaying the angle-resolved (AR) spectrum and the maximum intensity versus angle during the measurement (Live, AR spectrum, top). A degradation check allows to control of device degradation over the course of the measurement and to apply of an automatic correction if required (Degradation correction, bottom). The shown data is for the semi-transparent OLED design with dip-coated layers of PEDOT:PSS and SY-PPV.

The complete performance parameters of the best-performing devices for the semi-transparent and bottom-emitting device configurations are provided in Figure S8 (Supporting Information).

3. Conclusion

In conclusion, this study introduces two open-source tools designed to facilitate the fabrication and comprehensive characterization of thin film electronics, alongside an open-source software suite that streamlines OLED characterization within the framework of our previously presented open-source angle-resolved electroluminescence characterization setup. We present a dip-coating system for the manufacturing of different thin films, a four-point probe with a software package for the accurate determination of sheet resistances, and we show how these open-source systems can be used to fabricate, optimize, and characterize efficient OLED stacks.

The hardware solutions outlined herein represent a cost-effective alternative to commercial devices as they can be made from common lab equipment and affordable bespoke components. The main components required for the assembly of the dip coater can be purchased for ≈70 euros at the time of writing, whereas the parts required for the four-point probe can be obtained for less than 30 euros. In our experience, this costs 40 times and 80 times, respectively, lower than even the more cost-effective commercial alternatives. Moreover, additional support structures can be easily prepared by 3D printing. These economically viable solutions serve to further enhance accessibility to advanced tools for thin-film electronics research. Furthermore, this work describes a new software package for our previously established AR-EL characterization setup. This software empowers researchers to conduct thorough electroluminescence characterization and data analysis of OLEDs within a matter of minutes.

While the importance of publicly available projects is widely accepted in software development, open-source hardware lacks

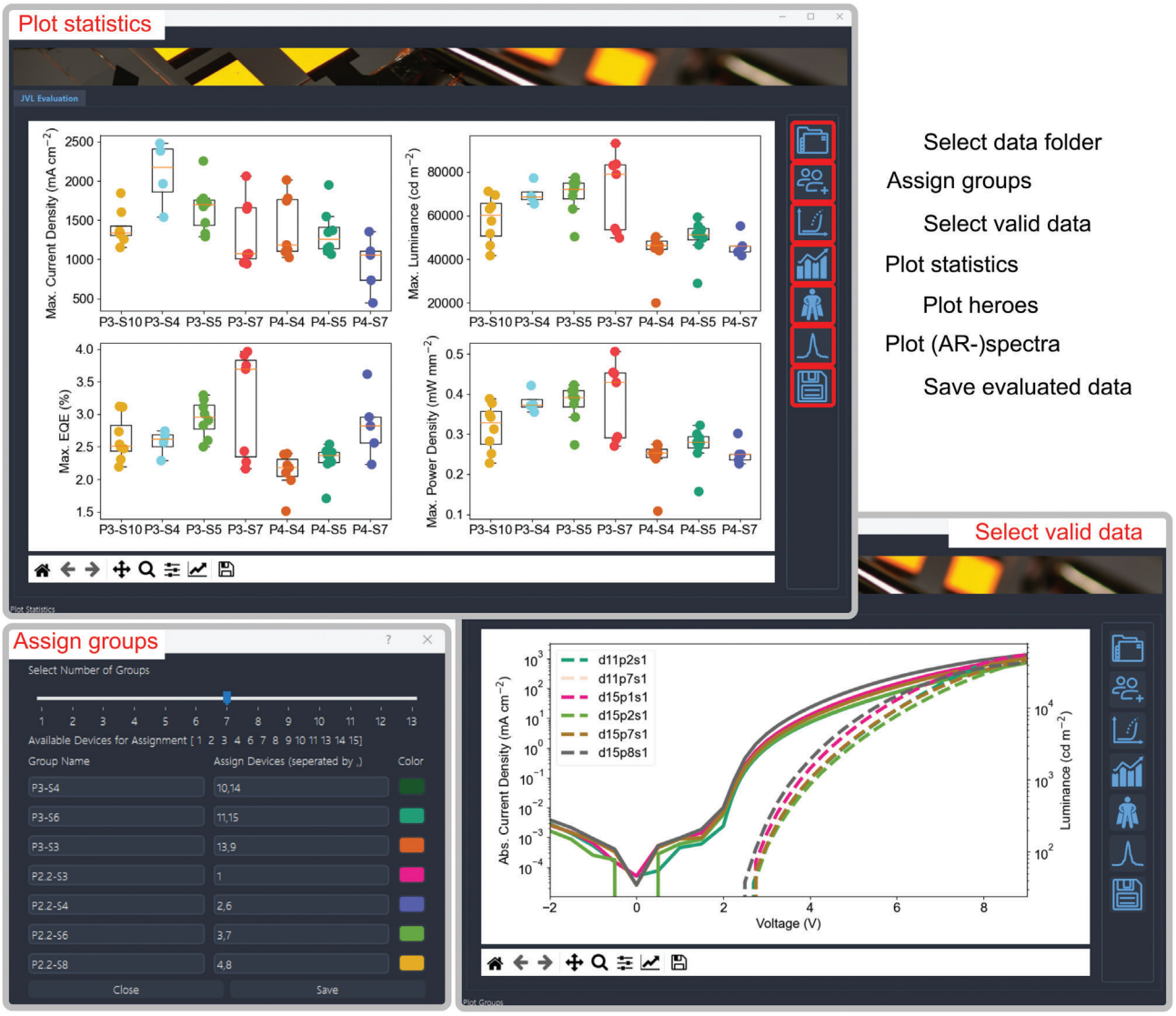

Figure 5. Software to evaluate the measured data and transform it into photometric and radiometric quantities. The shown data is for the opaque devices with dip-coated layers of PEDOT:PSS and SY-PPV with a thick aluminum electrode. After entering details about the measurement setup, device size, etc., the data can be loaded automatically from any folder. Subsequently, groups of devices with the same configuration can be defined and the data are transformed into photometric and radiometric quantities (Assign groups, bottom left). Afterward, any invalid data, e.g., from short pixels, can be rejected based on the displayed JVL curves (Select valid data, bottom right). Performance statistics for each device as well as for each previously defined group can be displayed to confirm the best device configuration within seconds (Plot statistics, top).

behind in some research areas. With the hardware and software specifically designed for thin film and organic electronics research that is introduced here, we hope to enhance accessibility, improve collaboration, and further advance the reproducibility of the data reported in our field. We also wish to inspire other researchers to share open-source versions of their custom designs in the future.

4. Experimental Section

Atomic Layer Deposition: Aluminum-doped zinc-oxide films were deposited via atomic layer deposition (Savannah S200; Veeco, USA) at different temperatures. Trimethylaluminum (TMA) (Strem, USA) pulses of 15 ms were followed by a 5 s purge time before injection of water for 15 ms and another 5 s waiting time. Each TMA + water pulse pair was followed by 20 pulses of water (15 ms + 10 s purge) + Diethyl-zinc (Strem, USA) (15 ms + 10 s purge time). This combination of pulses was repeated 32 times amounting to a total of 672 ALD cycles corresponding to ≈100 nm thickness.

Thermal Evaporation: Electrodes were fabricated by thermal evaporation via resistive sources in a high-vacuum environment (EVOVAC; Angstrom Engineering, Canada), maintaining a base pressure below 1×10^{-7} torr. The thickness of the deposited electrodes was measured using quartz crystal microbalances.

OLED Fabrication: Prepatterned ITO glass substrates (24 mm × 24 mm) (Xin Yan, Hongkong) were cleaned via sonication in deionized (DI) water, acetone, and isopropanol, each for 15 min. Next, PEDOT:PSS solution (poly(3,4-ethylenedioxythiophene):polystyrene

sulfonate; CLEVIOS P VP AI 4083) was filtered through a 0.45 µm PVDF membrane filter and mixed with DI water at a weight ratio of 1:2 to adjust its viscosity. For the hole injection layer, we dip-coated a 45–50 nm thick PEDOT:PSS layer onto the ITO-coated glass substrates. During this dip coating process, the retention time was set to 10 s, and then the retraction speed to 2.7 mm s^{-1}. The dip-coated PEDOT:PSS films were dried on a hotplate at 140 °C for 30 min. Subsequently, the devices were transferred to a nitrogen-filled glovebox to deposit the SY-PPV light-emitting layer. SY-PPV (Sigma-Aldrich) was dissolved in Chlorobenzene at 0.2 wt.% and retracted at different speeds to form layers of varying thickness, keeping a constant retention time of 10 s. The SY-PPV films were subsequently dried on a hotplate at 140 °C for 20 min. The samples were transferred to the vacuum chamber for thermal evaporation of the top contact without intermittent exposure to air. We deposited a 0.5 nm thick LiF layer, followed by either a 100 nm thick Al electrode for bottom-emitting devices or a 1 nm thick Al and 20 nm thick Ag electrode for semi-transparent devices. Before characterizing the devices, we removed the dip-coated layers on the back side of the substrate using acetone and DI water.

AFM Measurements: Atomic force microscopy measurements were performed using JPK Bruker The NanoWizard 4 mounted at the Nikon Ti2 optical microscope. Imaging was performed via frequency modulation; with the resonance frequency of the AFM probe $f_0 = 32$ kHz. All measurements were carried at room temperature.

Supporting Information

Supporting Information is available from the Wiley Online Library or from the author.

Acknowledgements

J.F.B. acknowledges funding from Beverly and Frank MacInnis via the University of St Andrews. This work was supported by the Alexander von Humboldt Foundation (Humboldt Professorship to M.C.G.), the DFG-funded Research Training Group "Template-Designed Organic Electronics (TIDE)" (RTG2591) and the Engineering and Physical Sciences Research Council (EP/X039250/1).

Conflict of Interest

The authors declare no conflict of interest.

Data Availability Statement

The data that support the findings of this study are openly available in University of St Andrews Repository at https://doi.org/10.17630/651679f3-4d56-40cd-b6da-e0c24804bcc3, reference number 305541831 and via Zenodo at https://doi.org/10.5281/zenodo.10546513 and https://doi.org/10.5281/10546515.

Keywords

characterization, fabrication, open-source, organic electronics, thin films

Received: June 13, 2024
Revised: July 15, 2024
Published online:

[1] H. Touvron, L. Martin, K. Stone, P. Albert, A. Almahairi, Y. Babaei, N. Bashlykov, S. Batra, P. Bhargava, S. Bhosale, D. Bikel, L. Blecher, C. C. Ferrer, M. Chen, G. Cucurull, D. Esiobu, J. Fernandes, J. Fu, W. Fu, B. Fuller, C. Gao, V. Goswami, N. Goyal, A. Hartshorn, S. Hosseini, R. Hou, H. Inan, M. Kardas, V. Kerkez, M. Khabsa, et al., *arXiv* **2023**, 09288.
[2] R. Rombach, A. Blattmann, D. Lorenz, P. Esser, B. Ommer. High-Resolution Image Synthesis with Latent Diffusion Models (Version 2). arXiv**2021**.
[3] B. Van der Zee, Y. Li, G. A. H. Wetzelaer, P. W. M. Blom, *Adv. Mat.* **2022**, *34*, 2108887.
[4] F. F. Voigt, D. Kirschenbaum, E. Platonova, S. Pagès, R. A. A. Campbell, R. Kastli, M. Schaettin, L. Egolf, A. van der Bourg, P. Bethge, K. Haenraets, N. Frézel, T. Topilko, P. Perin, D. Hillier, S. Hildebrand, A. Schueth, A. Roebroeck, B. Roska, E. T. Stoeckli, R. Pizzala, N. Renier, H. U. Zeilhofer, T. Karayannis, U. Ziegler, L. Batti, A. Holtmaat, C. Lüscher, A. Aguzzi, F. Helmchen, *Nat. Methods* **2019**, *16*, 1105.
[5] B. Wijnen, E. J. Hunt, G. C. Anzalone, J. M. Pearce, *PLoS One* **2014**, *9*, e107216.
[6] P. Slade, A. Akhtar, M. Nguyen, T. Bretl, in *2015 IEEE International Conference on Robotics and Automation (ICRA)*, IEEE, New York **2015**, pp. 6451–6456.
[7] D. Carbonell Rubio, W. Weber, E. Klotzsch, *HardwareX* **2022**, *11*, e00316.
[8] R. W. Bowman, *Nat. Rev. Methods Prim.* **2023**, *3*, 27.
[9] E. Hsiang, Z. Yang, Q. Yang, Y. Lan, S. Wu, *J. Soc. Inf. Disp.* **2021**, *29*, 446.
[10] C. Keum, C. Murawski, E. Archer, S. Kwon, A. Mischok, M. C. Gather, *Nat. Commun.* **2020**, *11*, 6250.
[11] J. Kim, J. Park, *Sci. Adv.* **2021**, *7*, eabd9715.
[12] T.-W. Lee, T. Noh, H.-W. Shin, O. Kwon, J.-J. Park, B.-K. Choi, M.-S. Kim, D. W. Shin, Y.-R. Kim, *Adv. Funct. Mater.* **2009**, *19*, 1625.
[13] Y. Chen, J. Wang, Z. Zhong, Z. Jiang, C. Song, Z. Hu, J. Peng, J. Wang, Y. Cao, *Org. Electron.* **2016**, *37*, 458.
[14] A. Strang, V. Quirós-Cordero, P. Grégoire, S. Pla, F. Fernández-Lázaro, Á. Sastre-Santos, C. Silva-Acuña, P. N. Stavrinou, N. Stingelin, *Adv. Mater.* **2023**, *36*, 2212056.
[15] S. Kwon, H. Kim, S. Choi, E. G. Jeong, D. Kim, S. Lee, H. S. Lee, Y. C. Seo, K. C. Choi, *Nano Lett.* **2018**, *18*, 347.
[16] E. Palo, M. A. Papachatzakis, A. Abdelmagid, H. Qureshi, M. Kumar, M. Salomäki, K. S. Daskalakis, *J. Phys. Chem. C.* **2023**, *127*, 14255.
[17] C. Sachse, L. Müller-Meskamp, L. Bormann, Y. H. Kim, F. Lehnert, A. Philipp, B. Beyer, K. Leo, *Org. Electron.* **2013**, *14*, 143.
[18] C.-S. Chou, F.-C. Chou, J.-Y. Kang, *Powder Technol.* **2012**, *215–216*, 38.
[19] J. F. Butscher, S. Hillebrandt, A. Mischok, A. Popczyk, J. H. H. Booth, M. C. Gather, *Sci. Adv.* **2024**, *10*, eadm7613.
[20] E. Guziewicz, M. Godlewski, L. Wachnicki, T. A. Krajewski, G. Luka, S. Gieraltowska, R. Jakiela, A. Stonert, W. Lisowski, M. Krawczyk, J. W. Sobczak, A. Jablonski, *Semicond. Sci. Technol.* **2012**, *27*, 074011.
[21] J. H. Im, K.-T. Kang, S. H. Lee, J. Y. Hwang, H. Kang, K. H. Cho, *Org. Electron.* **2016**, *33*, 116.
[22] M. Naftaly, S. Das, J. Gallop, K. Pan, F. Alkhalil, D. Kariyapperuma, S. Constant, C. Ramsdale, L. Hao, *Electronics (Basel)* **2021**, *10*, 960.
[23] A. Mischok, S. Hillebrandt, S. Kwon, M. C. Gather, *Nat. Photonics* **2023**, *17*, 393.
[24] E. Archer, S. Hillebrandt, C. Keum, C. Murawski, J. Murawski, F. Tenopala-Carmona, M. C. Gather, *Adv. Opt. Mater.* **2021**, *9*, 2000838.
[25] J. Puetz, M. A. Aegerter, *Sol-Gel Technologies for Glass Producers and Users*, Springer US, Boston, MA **2004**, pp. 37–48.
[26] L. Landau, B. Levich, *Dynamics of Curved Fronts*, Elsevier, Amsterdam **1988**, pp. 141–153.
[27] X. Tang, X. Yan, *J. Solgel Sci. Technol.* **2017**, *81*, 378.
[28] I. Miccoli, F. Edler, H. Pfnür, C. Tegenkamp, *J. Phys.: Condens. Matter* **2015**, *27*, 223201.

[29] H. Topsoe, *Geometric Factors in Four Point Resistivity Measurement*, **1968**.
[30] S. C. Gong, Y.-J. Choi, H. Kim, C.-S. Park, H.-H. Park, J. G. Jang, H. J. Chang, G. Y. Yeom, *J. Vac. Sci. Technol., A* **2013**, *31*, 01A101.
[31] H. Spreitzer, H. Becker, E. Kluge, W. Kreuder, H. Schenk, R. Demandt, H. Schoo, *Adv. Mater.* **1998**, *10*, 1340.
[32] R. Meerheim, K. Walzer, M. Pfeiffer, K. Leo, *Appl. Phys. Lett.* **2006**, *89*, 061111.
[33] C. Féry, B. Racine, D. Vaufrey, H. Doyeux, S. Cinà, *Appl. Phys. Lett.* **2005**, *87*, 213502.
[34] S. Burns, J. MacLeod, T. Trang Do, P. Sonar, S. D. Yambem, *Sci. Rep.* **2017**, *7*, 40805.